Retina

Enhanced S-Cone Syndrome: Elevated Cone Counts Confer Supernormal Visual Acuity in the S-Cone Pathway

Yiyi Wang,[1] Jessica Wong,[2] Jacque L. Duncan,[2] Austin Roorda,[1] and William S. Tuten[1]

[1]Herbert Wertheim School of Optometry and Vision Science, University of California, Berkeley, California, United States
[2]Department of Ophthalmology, University of California, San Francisco, California, United States

Correspondence: William S. Tuten, Herbert Wertheim School of Optometry and Vision Science, University of California, Berkeley, 412 Minor Addition, Berkeley, CA 94720, USA;
wtuten@berkeley.edu.

PURPOSE. To measure photoreceptor packing density and S-cone spatial resolution as a function of retinal eccentricity in patients with enhanced S-cone syndrome (ESCS) and to discuss the possible mechanisms supporting their supernormal S-cone acuity.

METHODS. We used an adaptive optics scanning laser ophthalmoscope (AOSLO) to characterize photoreceptor packing. A custom non-AO display channel was used to measure L/M- and S-cone–mediated visual acuity during AOSLO imaging. Acuity measurements were obtained using a four-alternative, forced-choice, tumbling E paradigm along the temporal meridian between the fovea and 4° eccentricity in five of six patients and in seven control subjects. L/M acuity was tested by presenting long-pass–filtered optotypes on a black background, excluding wavelengths to which S-cones are sensitive. S-cone isolation was achieved using a two-color, blue-on-yellow chromatic adaptation method that was validated on three control subjects.

RESULTS. Inter-cone spacing measurements revealed a near-uniform cone density profile (ranging from 0.9–1.5 arcmin spacing) throughout the macula in ESCS. For comparison, normal cone density decreases by a factor of 14 from the fovea to 6°. Cone spacing of ESCS subjects was higher than normal in the fovea and subnormal beyond 2°. Compared to the control subjects ($n = 7$), S-cone–mediated acuities in patients with ESCS were normal near the fovea and became increasingly supernormal with retinal eccentricity. Beyond 2°, S-cone acuities were superior to L/M-cone–mediated acuity in the ESCS cohort, a reversal of the trend observed in normal retinas.

CONCLUSIONS. Higher than normal parafoveal cone densities (presumably dominated by S-cones) confer better than normal S-cone–mediated acuity in ESCS subjects.

Keywords: retinal degeneration, visual acuity, adaptive optics retinal imaging, enhanced s-cone syndrome, NR2E3

In the normal human retina, rod and cone photoreceptors exhibit distinct topographical density profiles, the result of complex and finely orchestrated developmental processes that are initiated during gestation and continue postnatally.[1] Rods are absent at the foveola, and outside the fovea their packing density rises steadily with eccentricity, reaching a peak between 10° and 20° before declining again in the peripheral retina.[2,3] Despite the large number and high spatial density of rods, visual acuity is comparatively poor under scotopic conditions due to spatial convergence in rod-driven circuits.[3–5] Humans with normal color vision have three cone types that are sensitive to long, medium, and short wavelengths of light and are referred to as L-, M-, and S-cones, respectively. Like rods, S-cones are also excluded from the central fovea and follow a non-monotonic density profile, with a peak density occurring near 1° eccentricity.[6] S-cone proportion increases with eccentricity up to 10°[7] and comprises from 5% to 10% of the overall cone population, with L/M-cones making up the remaining 90% to 95%. L- and M-cones in the central retina are wired into specialized neural circuits canonically associated with high-resolution spatial vision,[8–12] whereas S-cones primarily feed into chromatic pathways with lower resolving capacity.[13–15] S-cones represent a mere ∼0.2% of all photoreceptors (rods plus cones) in normal eyes.

Enhanced S-cone syndrome (ESCS) is a rare inherited retinal degeneration in which photoreceptor differentiation is disrupted during development, and rod precursors are misdirected to form photoreceptors that express opsin typically associated with S-cones. ESCS was first described in 1989 with pathognomonic electroretinogram (ERG) findings, and its name came from the enhanced short-wavelength–sensitive cone function measured with ERG and psychophysics.[16–18] Together, these results point toward a supernormal complement of S-cones in patients with ESCS.[19–21]

ESCS is mostly associated with biallelic disease-causing variants in the nuclear receptor subfamily 2, group E, member 3 (*NR2E3*) gene, which encodes a transcription factor that promotes rod differentiation and suppresses the cone-expressing genes in the photoreceptor progenitor cells, as shown in the *rd7* mutant mouse, a model for human ESCS.[22] Other *NR2E3* gene mutations that solely affect rod photoreceptor transactivation result in autosomal dominant

1

retinitis pigmentosa (adRP) instead.[23] ESCS can also be associated with mutations in the neural retina leucine zipper (*NRL*) gene, a transcription factor upstream of *NR2E3*.[24,25] Biallelic pathogenic variants in the *NRL* or *NR2E3* gene misdirect rod precursors to produce S-cones.

Characterizing outer retinal cellular topography in ESCS is an important first step toward understanding the structural and functional consequences of disruptions to the regulatory networks that determine photoreceptor fate. In the simplest scenario, where precursor cells fated to become rods instead develop into S-cones and no other developmental processes are affected, the S-cone density profile should mirror that of rods in the normal retina, with supernormal cone densities outside the fovea. Postmortem findings from a 77-year-old ESCS donor eye confirmed the absence of rod photoreceptors and showed a twofold increase in overall cone density at a mid-peripheral retinal location (~15° nasal) analyzed via immunohistochemistry, with S-cones comprising 92% of the remaining photoreceptors.[26] More recently, high-resolution retinal imaging studies using adaptive optics have shown in a small number of subjects that the supernormal cone densities observed histologically are also present in vivo at eccentricities as low as 3°,[27,28] although overall cone counts at some parafoveal eccentricities were lower than the combined number of rods and cones that would normally be present in a healthy eye.[28] Furthermore, cone densities at the foveola, where S-cones and rods are excluded, were reduced compared to normal.[28] Currently, it remains unclear if the genetic mutations underlying ESCS also interfere with the development of the L/M-cone subsystem or if the reduced cone densities observed previously are the consequence of an ongoing diffuse degenerative process that causes cell loss in all extant receptor types.

The supernormal cone densities observed in these previous studies raise the intriguing possibility that patients with ESCS may, under certain conditions, be equipped with supernormal visual capacities. Realizing this possibility requires that the post-receptoral visual system can take advantage of the information encoded by the abnormally dense receptor array. Although prior studies have shown that the supernumerary complement of S-cones in ESCS confers improved performance on tasks such as contrast detection[21,29] and flicker perception,[30] the extent to which these benefits extend to the spatial domain is less clear. Greenstein and colleagues[29] measured S-cone–isolated grating acuity at 6° eccentricity in three patients with ESCS and reported a twofold improvement compared to normal, although the underlying receptor distribution at their test location was not known. In this study, we used a custom high-resolution retinal imaging and visual function testing platform to characterize cone topography across the central retina in ESCS while simultaneously measuring L/M- and S-cone–mediated visual acuity. Understanding the structure–function relationship in the ESCS retina could shed light on the potential benefits of *NR2E3* gene-related therapeutic treatments,[31–33] as well as the understanding of possible retinal remodeling during development when photoreceptors are abnormally distributed.

MATERIALS AND METHODS

Subjects

The retinal structure of six and function of five ESCS subjects were measured at University of California, San Francisco (UCSF). The results for the ESCS subjects were compared with those of normal subjects ($n = 7$) recruited and imaged at the University of California, Berkeley (UCB). All research procedures followed the tenets of the Declaration of Helsinki. Informed consent was obtained from all subjects after the purpose and possible consequences were explained. The research protocol was approved by the institutional review boards of UCSF and UCB.

All ESCS subjects had clinical eye examinations prior to the research imaging and consented to release their medical records. Full-field ERG testing in all subjects showed characteristic findings,[18] and genetic testing results revealed biallelic disease-causing variants in the *NR2E3* gene and confirmed the diagnosis of ESCS in all subjects. Best-corrected visual acuity was measured during clinical eye examination based on the Early Treatment of Diabetic Retinopathy Study (ETDRS) protocol.[34] Color vision was assessed in all subjects with the Farnsworth D-15 Dichotomous Color Blindness Test.[35] Cross-sectional scans of the retinas were obtained with spectral-domain optical coherence tomography (OCT; SPECTRALIS HRA+OCT system; Heidelberg Engineering, Heidelberg, Germany). For each subject, the eye with better appearing retinal integrity on OCT was selected for adaptive optics scanning laser ophthalmoscope (AOSLO) retinal imaging and psychophysical measurements. In some cases, AOSLO images of the fellow eye were also obtained, but time constraints prevented additional psychophysical testing. We did not recall subject 10055 for updated AOSLO imaging and psychophysical testing due to extensive retinal degeneration and poor visual acuity found in 2009.

High-Resolution Retinal Imaging and Analysis

All subjects were dilated with 1% tropicamide and 2.5% phenylephrine in both eyes before retinal imaging. AOSLO images of the retina were acquired using the systems at UCSF and UCB.[36,37] Both systems have similar optical design and identical software controls. Retinal videos (512 × 512 pixels) of ESCS subjects were acquired at 30 frames per second over a 1.2° × 1.2° field of view on the retina (0.9° × 0.9° field of view for normal subjects using the UCB system). We imaged ESCS subjects in the central 5° area and extended the horizontal meridians out to 8° eccentricity with the UCSF system, whereas normal subjects at UCB were imaged out to 4° along the temporal meridian where visual acuity was measured. High-resolution retinal images were generated offline with custom software after correcting for distortion caused by fixational eye movements.[38] All images at the macula and along the horizontal meridian were stitched together using Photoshop (Adobe, Mountain View, CA, USA) into a single montage using custom software.[39]

In each ESCS retinal montage in areas where contiguous arrays of cones were well resolved, 0.2° × 0.2° regions of interest (ROIs) were manually selected. Cone spacing was analyzed within these ROIs using custom software (Mosaic Analytics; Translational Imaging Innovations, Hickory, NC, USA) designed to analyze cell mosaics from AOSLO images, as previously described.[40] The *Z*-score value of the cone spacing of each ROI was reported as standard deviations from a normal database at the measured eccentricity.[41]

Measuring S- and L/M-Cone–Isolated Visual Acuity

S-cone isolation was achieved using a two-color, blue-on-yellow chromatic adaptation method, which leveraged the
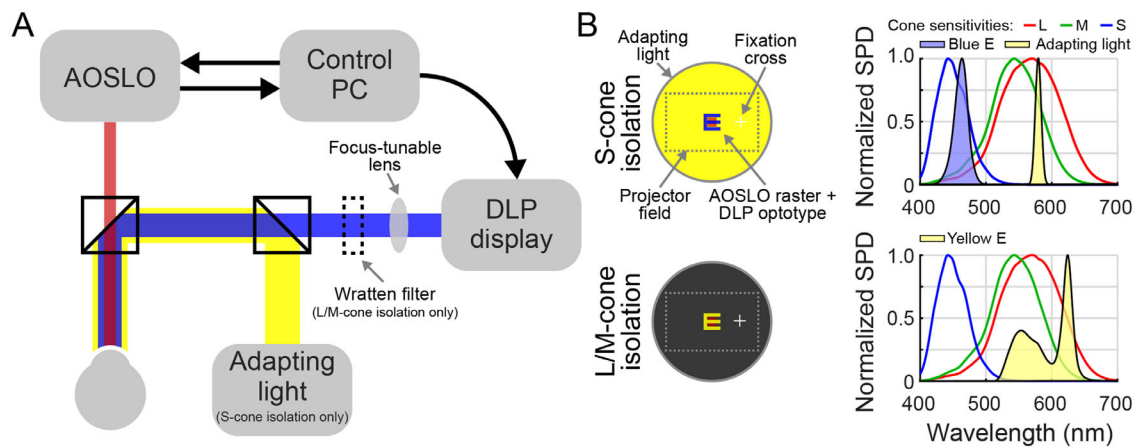
FIGURE 1. System schematic. (**A**) The psychophysical optotype E was delivered from the high-resolution Digital Light Processing (DLP) projector display through a different light path coaligned with the AOSLO beam. The focus of the letter E was adjusted with a focus-tunable lens subjectively. In the S-cone isolation condition, a background adapting light was created from an external light source coaligned with the projector path and AOSLO beam. The yellow adapting light was bright enough to desensitize the L/M-cones during S-cone acuity measurement. In the L/M-cone–isolating condition, a yellow letter E was created by filtering a white light through a long-pass Wratten 16 filter whose spectrum is outside of the sensitive region of the S-cones. (**B**) Cone isolation was achieved utilizing differences in spectral sensitivities.[85] In the S-cone–isolation condition, the subject viewed a blue letter E against a bright yellow background. In the L/M-cone–isolation condition, the subject viewed a yellow letter E against a black background. The red AOSLO IR raster was present and centered with the letter in both conditions.

distinct spectral sensitivities of the S- and L/M-cone types to suppress the sensitivity of L/M-cones while preserving S-cone contrast (Fig. 1A).[13,42] A modified high-resolution (136 pixels/deg) Digital Light Processing (DLP) projector (TI DLP LightCrafter 4500; Texas Instruments, Dallas, TX, USA) was used to present the blue S-cone–isolating letter E in a Maxwellian view configuration. The spectral power distribution of the DLP blue primary is shown in Figure 1B. The focus of the DLP display was controlled by an electrically tunable liquid lens (EL-3-10; Optotune Switzerland AG, Dietikon, Switzerland) placed in a plane conjugate to the subject's pupil; the aperture of the liquid lens formed a 2.5-mm artificial pupil through which the subject viewed the acuity stimulus. The focus of the DLP display was adjusted manually by the experimenter while the subject judged the sharpness of an ETDRS acuity chart rendered with the blue projector primary. A cylindrical trial lens was placed adjacent to the liquid lens to correct for any residual astigmatism based on the subject's refractive error.

To create a long-wavelength adapting background, broadband light from a fiberoptic illuminator source was passed through a narrowband filter (λ_{center} = 580 nm, FB580-10; Thorlabs, Newton, NJ, USA) (Fig. 1B) and delivered to the retina in Maxwellian view; the adapting field subtended approximately 18° and was coaligned to the projector display and AOSLO imaging raster. The luminance of the stimulus and adapting channels was measured using a spectroradiometer (PR-650 Spectra Scan; Photo Research, Chatsworth, CA, USA). On average, the luminance of the projector with blue stimulus was 21.4 cd/m², and the yellow background was set to be ≥6,400 cd/m² to produce the ≥300:1 luminance ratio previously demonstrated to achieve S-cone isolation.[42] Pilot measurements obtained from control subjects at UCB confirmed that blue-on-yellow acuity performance plateaued at a similar luminance ratio in our apparatus, indicative of S-cone isolation.

Prior to data collection, all study participants completed a practice run of 15 trials following the procedures described below. These trials were intended to familiarize participants

with the experimental procedure and were discarded from subsequent analyses. At the beginning of each block of trials, the subject first aligned a reticle target presented in the DLP display to the AOSLO imaging raster. This step ensured that DLP stimuli could be presented spatially coincident to the imaging raster, thereby permitting the recovery of the retinal location stimulated on each trial by analyzing retinal videos recording during the experiment (see below). Next, the subject adapted for 60 seconds to the yellow background to induce adaptation in L/M-cones. When the adaptation period concluded, visual acuity was measured using a four-alternative, forced-choice (4AFC) tumbling-E paradigm. Each trial consisted of a 1-second interval during which a blue letter E was presented for 200 ms (n = 4) or 500 ms (n = 1; see below) against the bright yellow background. We note that subject 40234, whose clinical acuities were reduced due to macular edema, required a longer stimulus duration (500 ms) to reliably detect the acuity stimulus. Targeted retinal locations were selected for acuity testing along the temporal meridian between the fovea and 4° eccentricity in 1° increments. At each eccentricity, acuity was estimated using two 25-trial QUEST staircases collected in succession.[43] Staircase data were then fit with a psychometric function[44] to determine the threshold letter size at which the subject was able to correctly identify its orientation 62.5% of the time. The subject initiated each trial and submitted their responses via keypress. All experimental procedures were written in MATLAB (MathWorks, Natick, MA, USA) using routines available in the Psychtoolbox.[45]

Because ESCS is a degenerative condition that could produce an overall reduction in visual acuity, L/M-cone–isolated acuities were also measured at each test location to serve as a control against which S-cone acuities could be compared. L/M-cone acuities were obtained following the procedures described above with two exceptions. First, no adapting light was used to suppress the sensitivity of a particular cone class. Second, a yellow optotype was created by filtering a white letter E from the projector system with a long-pass filter (Wratten 16; Eastman Kodak Company,

Rochester, NY, USA) to create a stimulus that excluded the part of the spectrum to which S-cones are sensitive. The focus of the DLP display arm was adjusted to optimize the sharpness of a white ETDRS chart viewed through this filter. The mean luminance of the yellow E stimulus was 368 cd/m^2, and its spectral power distribution is shown in the lower right panel of Figure 1B.

The targets used to control fixation depended on test eccentricity but were otherwise kept consistent between measurement conditions and subject groups. When measuring acuities away from the fovea, a white square (20 × 20 arcmin) delivered via the projector display was used as a fixation marker. A relatively large marker was chosen to ensure visibility when the bright yellow adapting field was present. For foveal measurements, a large (∼3° × 3°) white square outline was presented concentric to the AOSLO imaging raster; the subject was instructed to fixate at the center of this box during the foveal task.

For all test conditions, a 1-second AOSLO video was recorded concurrently with each psychophysical trial. To synchronize the image acquisition with stimulus presentation on the DLP, a digital marker was added to the AOSLO video frames corresponding to the onset and offset of the acuity stimulus delivered via the projector. AOSLO video frames on which the DLP stimulus was present were extracted and combined into a master video file for each test condition and eccentricity. A reference frame was manually selected from this master video, and all other frames were registered to it with the cross-correlation function in MATLAB; the displacements required to register frames in the master video provided an estimate of eye position during stimulus delivery. An isoline contour analysis algorithm was used to determine the retinal region that encircled 68% of the stimulus deliveries.[46,47] The isoline contour image was then aligned manually to the AOSLO image montage generated as described in the preceding section.

RESULTS

Structural Analysis

Six ESCS patients had retinal eye examinations, and five of them underwent high-resolution retinal imaging along with visual psychophysics in 2021 and 2022. The detailed subject profile is shown in the Table. OCT scans showed abnormal lamination in the outer nuclear layer in all of the ESCS patients and cystoid spaces in both eyes of 40231 and 40234, as well as in the right eye of 40188 (Fig. 2), similar to findings reported previously.[48–50] In eyes without macular edema, the foveal pit appeared normal even though the photoreceptor packing in and around the fovea was atypical.

Cone spacing was measured from manually selected regions in the AOSLO images that had contiguous mosaics of unambiguous cones. However, the mosaics in the ESCS patients were not uniform, containing regions with no discernable cones (Fig. 3). This could reflect cone degeneration (supported by nonuniformity of the photoreceptor lamination in the OCT images), reduced cone reflectivity, or shadows and scattering from edema and the boundaries of the cystoid spaces in the inner retina. Given this uncertainty, one should not use local spacing estimates to infer total cone counts; rather, the cone spacing represents the local maximum density at each eccentricity (Fig. 4A).

Figure 4A shows the cone spacing as a function of eccentricity for 40 normal eyes[41] and the seven ESCS eyes. In normal subjects, cone spacing increases with eccentricity, as cone density declines. Cone spacing in five ESCS subjects was higher in the fovea than normal but remained uniform with increasing eccentricity, with lower than normal cone spacing (higher cone density) outside of the fovea. Subject 10055 had increased cone spacing (lower cone density) within 2° of the macula due to more advanced retinal degeneration, but the cone spacing fell within the normal range beginning 3° from the fovea. In the remaining subjects, the majority of cone spacing measurements fell between 1.0 and 1.5 arcmin. Using a previously described approach,[8] their cone spacing corresponds to a Nyquist sampling limit of 0.87 and 1.30 arcmin, respectively, for a hexagonally packed cone mosaic. These values correspond to Snellen acuities of 20/17 and 20/25, respectively. To compare the ESCS cone spacing profile with normal subjects, Figure 4B shows the *Z*-scores of the cone spacing in ESCS subjects across different eccentricities. The *Z*-score values are below zero beyond 2° eccentricity in five subjects. Subject 10055L had a higher than normal *Z*-score around the fovea (outside of the *y*-axis range

TABLE. Demographic Information and Clinical Data for Six ESCS Subjects

Subject	Exam Year	Age (Y)	Gender	Genetics	Visual Acuity	Color Vision	Note
10055	2009	59	Female	*NR2E3:* c.373C>T (p.Arg125Ter) *NR2E3:* c.626dup (p.Tyr209Ter)	OD/OS 20/200	Not measured	—
10054	2009	35	Male	*NR2E3:* c.229C>T (p.Arg77Trp)	OD/OS 20/32	Normal	Nephew of 10055
	2022	48		*NR2E3:* c.373C>T (p.Arg125Ter)	OD 20/32^{-1} OS 20/40^{-1}	Normal	
40188	2019	19	Female	*NR2E3*: c.932G>A (p.Arg311Gln) homozygous	OD/OS 20/20	Normal	—
	2021	21			OD 20/16^{-2} OS 20/20^{+1}		
40231	2021	22	Male	*NR2E3*: c.932G>A (p.Arg311Gln) homozygous	OD 20/30^{+2} OS 20/40^{+2}	Normal	—
40234	2022	20	Female	*NR2E3*: c.932G>A (p.Arg311Gln) homozygous	OD 20/60^{-} OS 20/40	Normal	Sister of 40231
40133	2015	16	Male	*NR2E3:* c.702G>A, p.(Trp234*)	OD/OS 20/25	Normal	—
	2021	22		*NR2E3:* c.223G>T (p.Val75Leu) VUS	OD/OS 20/25		

The age, genetics, visual acuity, and color vision results were from the clinical eye examination of the corresponding years. The visual acuities of the right eye (OD) and left eye (OS) were reported separately when they were different, and only one single acuity was shown when each eye had the same acuity.
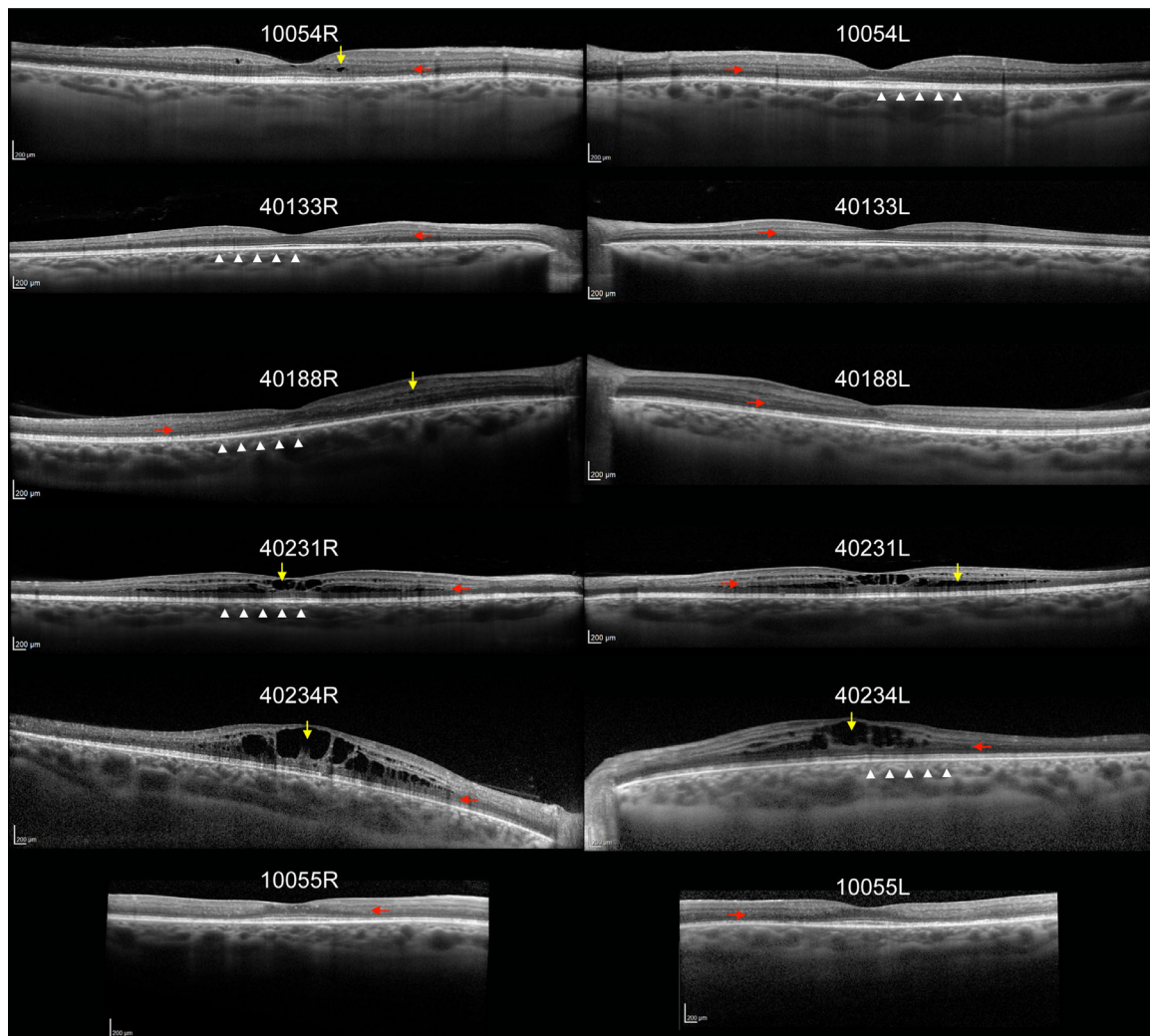
Figure 2. OCT images of six ESCS subjects. Both eyes of all subjects are shown. Each OCT scan was 30° except for subject 10055 (20°). All subjects showed abnormal retinal lamination in the outer nuclear layer where an additional hyperreflective band (indicated by *red arrows*) was observed, possibly representing an abnormally visible Henle's fiber layer.[27] Subjects 10054R, 40188R, 40231R&L, and 40234R&L showed intraretinal cysts (indicated by *yellow arrows*). Five eyes of six subjects were measured with cone-type–mediated acuity, and the presumed test locations are indicated by the *white arrowheads* from fovea to 4° temporal retina.

of Figure 4B) but normal *Z*-scores at eccentricities greater than 2°.

S- and L/M-Cone–Isolated Visual Acuity

AOSLO retinal images obtained simultaneously with psychophysical testing allow us to recover the trial-by-trial location of stimulus delivery for each test condition from the fovea to 4° eccentricity in the temporal retina (Fig. 3). Although stimulus delivery through the DLP projector was not contingent on eye position, the regular spacing of the isoline contours confirmed that subjects were maintaining their gaze on the fixation target during the psychophysical task, and acuity measures were obtained at the intended eccentricities. Moreover, the stimuli in both conditions appeared to be landing on the same part of the retina at all eccentricities except for the fovea, where S-cone–isolating conditions tended to produce larger and sometimes displaced fixation patterns. A similar trend was observed in the foveal S-cone–isolating data from normal

subjects (Fig. 3, top row) and may reflect a behavioral adaptation to the absence of S-cones in the central fovea.[6] Due to poor retinal video quality along the horizontal meridians in 40231R from intraretinal cysts, the eye positions of 40231R were not analyzable and thus the retinal images with incomplete fixation plots were not shown in Figure 3.

Figure 5A shows the average L/M-cone acuity as a function of retinal eccentricity in seven normal subjects and five subjects with ESCS. In all seven normal subjects, L/M-cone acuity was 20/20 or better at the fovea and declined with increasing eccentricity, consistent with previous findings.[8,51] In the ESCS cohort, the average L/M-mediated acuity was about 20/60 at the fovea and exhibited a monotonic decline across the parafovea, approaching near-normal levels by 4° eccentricity (Fig. 5A).

The relationship between S-cone–isolating acuity and retinal eccentricity is shown in Figure 5B. In normal subjects, the average S-cone acuity was about 20/200 at the fovea and 1° eccentricity and then declined slightly to 20/300 by
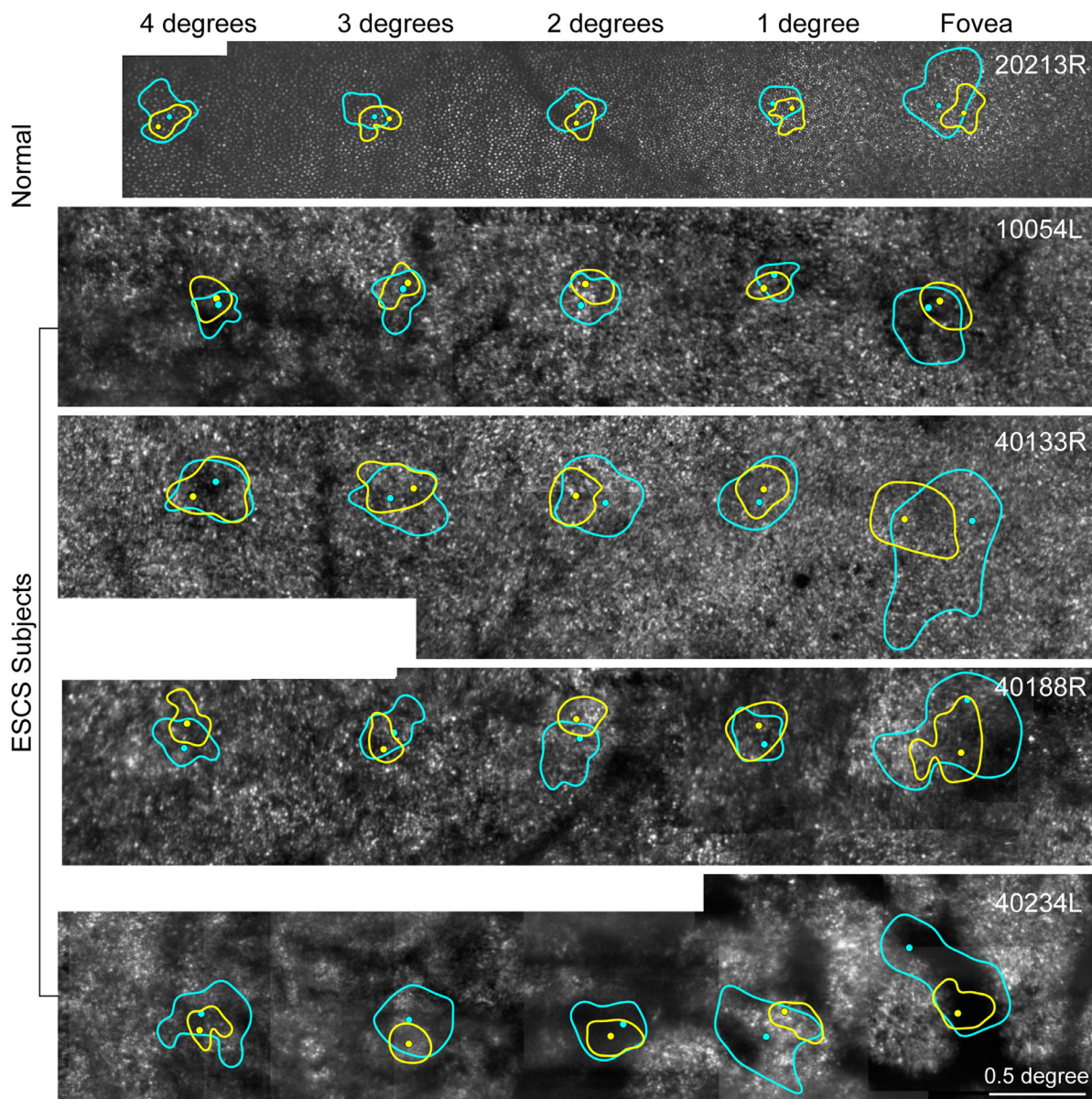
FIGURE 3. AOSLO confocal images with fixation behavior contours during acuity tasks. Each image shows a patch of retina from the fovea to 4° temporal retina. The images of subjects 10054L and 40234L are horizontally mirrored to position the fovea on the right side. The *white bar* indicates a 0.5° scale. *Yellow* and *cyan contours* show 68% fixation distribution from the L/M-cone and the S-cone acuity task, respectively. Within each contour, *one large dot* indicates the mean fixation location.

4° eccentricity. The S-cone acuity results we obtained at the fovea agree well with previous measurements in normal subjects.[13] By contrast, S-cone acuities in the patients with ESCS were near normal at the fovea and improved steadily with increasing eccentricity. At 4°, ESCS patients performed nearly three times better than normal subjects measured under the same conditions (Fig. 5B). In fact, the average S-cone acuity for ESCS subjects (20/107) was similar to the mean L/M-cone acuity in normal subjects (20/90) at the 4° location, whereas S-cone acuity in normal subjects at 4° was reduced to 20/300.

To compare our subjects' performance more quantitatively across the tested eccentricities, we show performance ratios between test conditions (S- vs. L/M-cone acuity) (Fig. 5C) and between subject groups (ESCS vs. normal)

(Fig. 5D). Figure 5C shows the $\log_{10}$ acuity ratio of S-cone acuity against the L/M-cone acuity for normal subjects (open circles) and patients with ESCS (black diamonds). Data below the horizontal zero line indicate that S-cone acuity was worse than L/M-cone acuity, whereas points above the zero line correspond to locations where S-cone acuity was superior to that mediated by L/M-cones. As expected, normal subjects had worse S-cone acuity than L/M-cone acuity at all eccentricities we measured, consistent with the idea that L- and M-cones provide the primary inputs to retinal pathways involved in high-acuity vision.[9–12] By contrast, in ESCS subjects, the discrepancy between L/M- and S-cone mediated acuity in the central fovea was smaller, and beyond 2° eccentricity the S-cone pathway slightly outperformed its L/M counterpart. Together, these data suggest that S-cones make
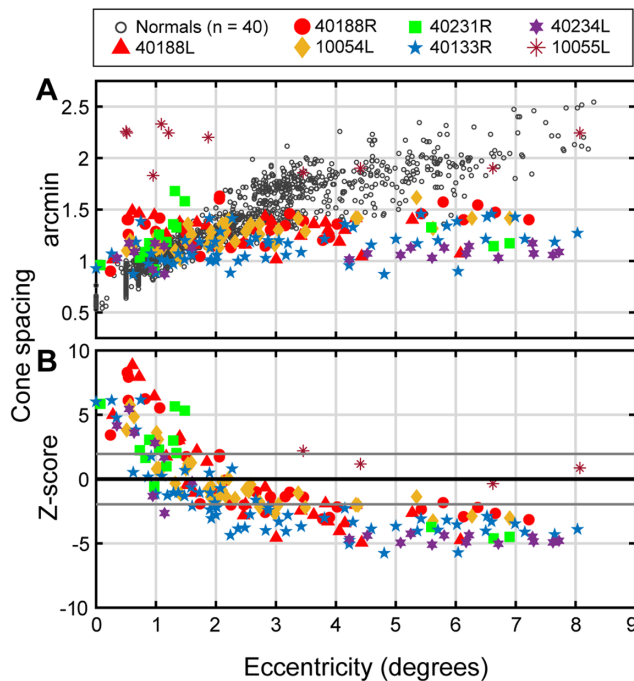
FIGURE 4. (**A**) Cone spacing as a function of retinal eccentricity. Normal data[36,41] are plotted with *black circles* on a common eccentricity axis. (**B**) Cone spacing *Z*-score as a function of retinal eccentricity. The *Z*-scores are computed considering retinal locations at four major meridians.[41] The *horizontal zero line* shows a *Z*-score of 0, and the *gray lines* show ±1.96 SD from the mean (95% confidence interval). Cone spacing *Z*-scores outside of the *y*-axis range (all of which came from subject 10055) are not shown in the plot.

a greater contribution to the pathways subserving spatial vision throughout the central retina in ESCS.

Figure 5D quantifies ESCS performance relative to normal for the S- and L/M-cone–mediated acuity tasks. Near the fovea, S-cone acuity was similar across the two groups, whereas L/M-cone acuity was significantly diminished in ESCS compared to normal. At 4° eccentricity, however, the disparity in L/M-cone performance between the two groups appeared to be less severe, and patients with ESCS exhibited supernormal S-cone acuity. Finally, to illustrate qualitatively how the relationship between structure and function varied between normal subjects and patients with ESCS, Figure 6 shows how threshold E letter size for the two cone-isolating conditions scaled with the outer retinal structure for exemplary subjects from each cohort.

We note here that our L/M-cone acuities measured at the fovea in ESCS were generally lower than the corresponding clinical acuities reported in the Table, although differences in measurement conditions may have contributed to the discrepancies in the performance we observed. Specifically, the acuity stimuli used in the experimental and clinical measurements differed in their spectral content (S-cone–excluding vs. broadband), temporal characteristics (200 ms presentation vs. unlimited viewing), and spatial frequency composition (similar Fourier spectra in the 4AFC task vs. more varied spectra in the ETDRS optotypes[52]). Subjects 40231 and 40234 had bilateral macular edema, shown in Figure 2, which could have contributed to the poorer L/M-cone foveal acuities compared to the other three subjects with relatively less disrupted foveal architecture (Table).

DISCUSSION

Although all inherited retinal degenerations are characterized by a progressive loss of one or more specific visual functions, ESCS is unusual in the sense that its atypical phenotype also has the potential to confer a gain in function along another dimension of human vision. We confirm the findings from previous histological[26] and imaging studies[27,28] supporting the notion that ESCS retinas are equipped with a surplus of S-cone–like photoreceptors (at the expense of rods and thus scotopic vision). A detailed understanding, however, of how younger patients with ESCS capitalize on this excess number of S-cones has until now remained largely unknown, particularly at the cellular scale. Specifically, the functional consequences associated with this unusual phenotype have been studied primarily using electroretinographic[16,18,53,54] and psychophysical perimetric techniques,[17,20,21,55] which provide no information about how, or whether, post-excitation mechanisms might leverage the supernormal complement of cones to improve spatial vision.

In this study, we combined high-resolution adaptive optics retinal imaging with simultaneous visual function testing to examine cone topography and spatial vision across the fovea and parafovea in ESCS. Our imaging results revealed subnormal cone densities occurring within the central 2° and supernormal cone densities beyond 2°, out as far as 8° (Fig. 4A). For L/M-cone–mediated acuity, the largest difference between our study groups was observed at the fovea, where patients with ESCS performed roughly threefold worse than the control group (Fig. 5A). For S-cone–mediated acuity, the ESCS and control groups performed similarly at the fovea and 1°. At greater eccentricities, performance between the two groups diverged, with patients with ESCS exhibiting increasingly supernormal acuities out to the largest eccentricity studied (4°) (Fig. 5B). This finding extends the results of Greenstein and colleagues,[29] who found a twofold improvement in S-cone grating acuity at 6° eccentricity in a group of three patients with ESCS whose cone mosaic topography was unknown. Below we discuss the implications of our results for receptoral and postreceptoral organization in ESCS.

Arrangement of L/M- and S-Cone Submosaics

Although the abundance of S-cones in the retinas of ESCS patients is well established, the organization of L/M- and S-cone submosaics is less clear, particularly in and around the fovea. Young patients with ESCS often have normal color vision, which suggests that L/M-cones are present in some number.[53] Clinical visual acuity measurements in ESCS are highly variable among subjects, ranging from 20/20 to 20/1000, depending on different disease stages.[50] In the normal retina, L/M-cones are concentrated in the foveal center, and acuity is ultimately limited by the L/M-cone mosaic sampling. AOSLO imaging showed reduced foveal cone densities in our ESCS subjects (Fig. 4), presumably due to reduced densities of L/M-cones. The reduced photoreceptor density we observed in our retinal images is consistent with the slightly reduced foveal L/M-mediated visual acuities in our ESCS subjects without macular edema (10054, 40133, and 40188) (Table). Unlike L/M-cone acuity, foveal measurements of S-cone acuity in the ESCS group were similar to the normal cohort (Fig. 5B), suggesting that ESCS retinas develop an S-cone–free foveola similar to that found in
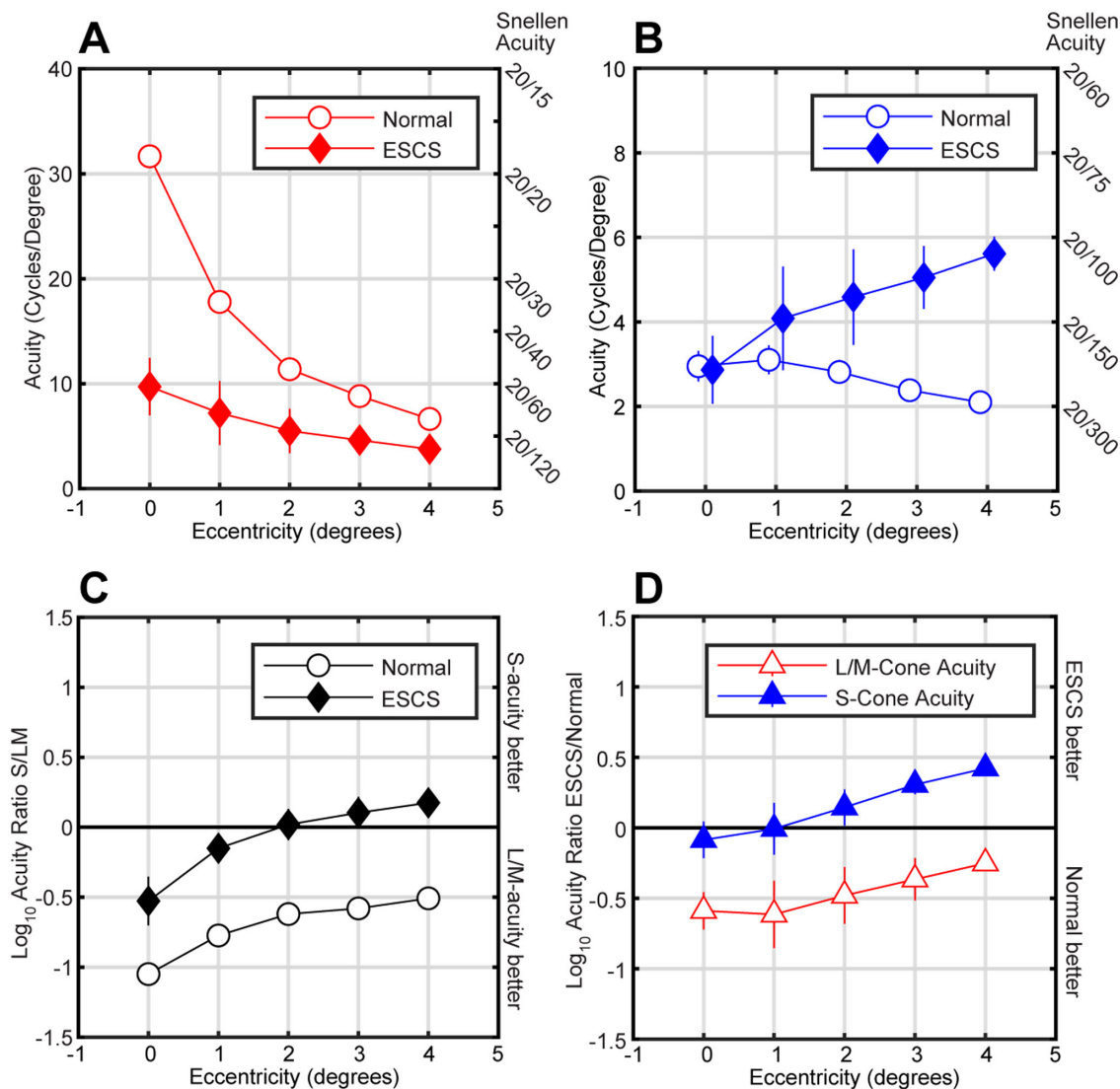
FIGURE 5. (**A**) L/M-cone acuity performance as a function of retinal eccentricity in ESCS and normal subjects. *Red open circles* show L/M-cone acuity in seven normal subjects and *red diamonds* show averaged L/M-cone acuity in five ESCS subjects. *Error bars* are standard errors of the mean. (**B**) S-cone acuity performance as a function of retinal eccentricity in ESCS and normal subjects. The *y*-axis is adjusted to show the low-spatial-frequency region, and data are shifted laterally to minimize overlap. *Blue open circles* show S-cone acuity in seven normal subjects, and the *blue diamonds* represent averaged S-cone acuity in five ESCS subjects. *Error bars* are standard errors of the mean. (**C**) Log_{10} acuity ratio as a function of retinal eccentricity in ESCS and normal subjects. The *horizontal zero line* represents equal S-cone and L/M-cone acuity. The area above the *horizontal zero line* shows when S-cone acuity was better than L/M-cone acuity at the targeted eccentricity. *Error bars* are standard errors of the mean. (**D**) Normalized log_{10} acuity ratio in cycles per degree. The *horizontal zero line* represents equal acuity in ESCS and normal subjects. The area above the *horizontal zero line* shows when ESCS acuity was better than that for normal subjects.

normal eyes. Collectively, our imaging and psychophysical results imply that the central fovea in ESCS is characterized by an overall reduction in cone density but features an otherwise normal spectral topography.

Away from the foveal center, L/M-mediated acuity was also worse in the ESCS group compared to normal, although the two curves appeared to converge with increasing eccentricity (Figs. 5A, 5D). Although it is tempting to view this confluence as evidence of a relatively normal parafoveal L/M mosaic, it is important to point out that visual acuity at these eccentricities is likely limited by spatial pooling in the midget retinal ganglion cell (mRGC) pathway rather than by the packing density of the cone mosaic.[8] As such, our imaging and psychophysical results do not exclude the possibility that the cone density of the parafoveal L/M-cone submosaic is also reduced. Whether the reduced L/M-cone

densities suggested by our data exist from birth or are the consequence of ongoing degeneration is not known, although the progressive loss of L/M-cone function observed in longitudinal perimetry studies supports the latter interpretation.[21] In contrast to L/M-cone acuity, S-cone acuities in the ESCS group became increasingly supernormal with increasing eccentricity (Fig. 5B), presumably due to the rise in cone numbers we observed via high-resolution imaging (Figs. 3, 4).

The fact that the elevated cone counts in ESCS did not extend to the foveal center is consistent with the histological finding that rod precursors are already excluded from the incipient fovea when the earliest expression of *NR2E3* occurs around fetal week 12.[56] The apparently limited role in *NR2E3* for foveal specialization is consistent with a framework wherein the development of the normal trichromatic cone
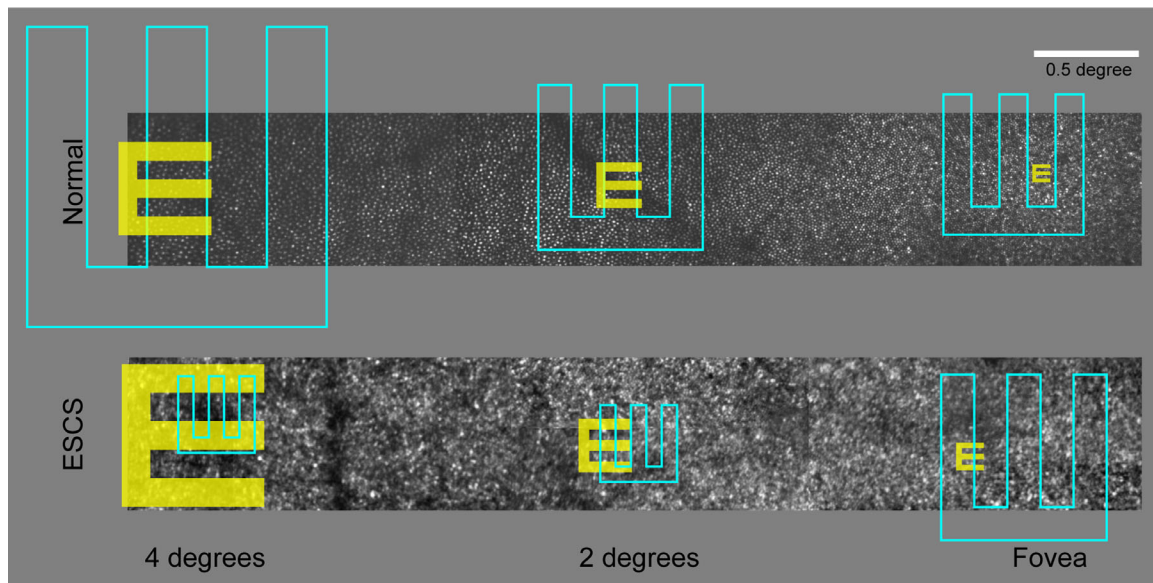
FIGURE 6. AOSLO confocal images with acuity locations of one normal (*upper panel*) and one ESCS subject (*lower panel*). From right to left shows fovea to 4° temporal retina. The *white bar* shows 0.5° scale. The acuity threshold letter sizes of each retinal location and S- and L/M-cone–isolating condition are represented by the *cyan* and *yellow letters*, respectively. Each letter E is centered at the stimulus delivery location. In the normal eye, L/M-cone threshold letter size (*yellow*) was small at the fovea and increased with eccentricity; a similar trend was seen in the S-cone task, but the S-cone threshold letter size (*cyan*) was significantly larger. In an ESCS subject, the L/M-cone acuity threshold size was slightly larger than normal but followed the same trend. Most noticeably, the S-cone acuity of this ESCS subject was worse than normal at the fovea but gradually improved from 1° to 4° eccentricity, showing the exact opposite trend as normal S-cone acuity.

mosaic is initiated prior to rod precursors being misdirected to form the surplus S-cones. This leads to the prediction that the excess S-cones fill in the band of retinal eccentricities normally inhabited by rods. Our data are broadly consistent with this view, which is also supported by previous work showing that cone photoreceptors develop before rods,[57,58] that the *NR2E3* expression pattern follows the eccentricities normally occupied by rods,[21] and that the topography of S-cone sensitivity in ESCS subjects resembles that of the normal rod system.[17,54] Whether the genetic mutations that underpin ESCS interfere with foveal photoreceptor development could be clarified by applying in vivo imaging techniques to characterize cone packing in younger carriers of *NR2E3* mutations, whose retinas would presumably be less affected by degeneration. If foveal cone density is normal in younger patients with ESCS, that would suggest the primordial cone mosaic develops normally but is then afflicted with degeneration secondary to the aberrant development of rod precursors.

The measurements of cone spacing we derived from our retinal images enabled us to estimate local cone counts and, by extension, to place bounds on the relative increase in S-cone numbers found in the ESCS retina. Assuming hexagonal cone packing and varying degrees of degeneration of the L/M-cone submosaic, we estimated the overall S-cone percentage and S-cone increase (relative to normal S-cone counts) in ESCS at each eccentricity based on a normal database and previously reported methods.[6,8,36,41] In the normal eye, S-cones make up 5% to 7% of the cone mosaic at the non-foveal eccentricities studied here.[6] By contrast, if no degeneration of the L/M-cone mosaic is assumed in ESCS retinas, we estimate that S-cones constitute 22% of the cone mosaic at 2°; by 7° eccentricity, this number rises to 68% of the receptor array (Fig. 7A). Note that these estimates of S-cone percentage should be considered a lower bound

because they assume the supernormal cone counts we estimated from our AOSLO images reflect a normal number of L/M cones plus an abnormally high number of S-cones; any loss of the L/M-cone mosaic due to degeneration would require even higher S-cone percentages to account for the elevated cone numbers we observed. For comparison, the ESCS histology study reported a 92% S-cone percentage and an abnormally reduced number of L/M-cones.[26] Because ESCS retinas exhibit supernormal parafoveal cone densities, the increases in S-cone numbers relative to normal counts are even more striking: At 7° eccentricity, we estimate the increase in S-cones to be anywhere from 26-fold (assuming no L/M degeneration) to 65-fold (assuming a uniform 50% cone degeneration) (Fig. 7B). These estimates lie within the wide range reported in the literature, including an 11-fold increase estimated from the temporal acuity study[30] and a 75-fold increase derived from analysis of full-field ERG responses.[54]

What Is Mediating S-Cone Acuity?

The S-cone acuities obtained from the control subjects in our study are broadly consistent with previous measurements in which a similar blue-on-yellow chromatic adaptation method was used to isolate S-cones.[13,42,59,60] Although under normal circumstances the S-cone submosaic is sparsely distributed, S-cone acuity falls well below the sampling limit imposed in the outer retina, implying that resolution in the S-cone pathway is instead limited by the spatial density of post-receptoral neurons—most likely the small bistratified retinal ganglion cells (sbRGCs) that receive direct excitatory input from multiple S-cones.[6,13,15,61] In ESCS, we observed a supernormal number of cone photoreceptors, the bulk of which are presumably S-cones, and a resultant increase in S-cone–mediated acuity. The neural basis for
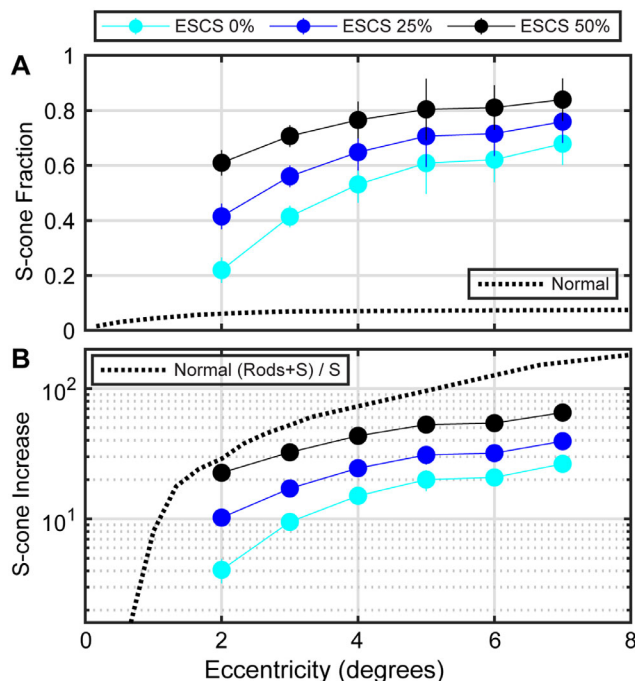
FIGURE 7. (**A**) S-cone percentage as a function of retinal eccentricity in different levels of degeneration in the L/M-cone mosaic. Normal S-cone percentage is shown in the *black dashed curve* from normal S-cone topography data.[6] ESCS subjects showed significantly higher S-cone density across all eccentricities modeled with 0% L/M-cone degeneration (*cyan*), 25% L/M-cone degeneration (*blue*), and 50% L/M-cone degeneration (*black*). (**B**) S-cone density increased as a function of eccentricity with the different degrees of L/M-cone degeneration described in (**A**). Assuming no degeneration, S-cones were increased 28-fold at 7° eccentricity in the ESCS subjects. Also, with 50% cone degeneration, the S-cones at 7° were increased by 65-fold. If all of the rods became S-cones, the maximum ratio of the S-cone density increase is shown in the *black dashed curve* calculated from normal photoreceptor topography.[2,6] *Error bars* are standard errors of the mean.

this enhanced resolving capacity is not known, although it implies a departure from how S-cone signals are normally processed by post-excitation mechanisms. Here, we present three hypotheses for how supernormal spatial vision in ESCS may arise.

Small Bistratified Retinal Ganglion Cell Pathway. The sampling limit of the sbRGC mosaic has been shown to agree well with S-cone acuity measurements obtained from 0° to 40° eccentricity.[13] If the same pathway supported the supernormal S-cone acuity we observed in ESCS subjects, there would have to be a concomitant increase in sbRGC density. Such an increase of sbRGCs in ESCS subjects was previously suggested[29] but not confirmed. Although visual experiences seem to shape the synaptic connections established during retinal development,[62] it has also been shown that RGCs develop before photoreceptors and bipolar cells,[63] and RGCs can maintain normal morphology and projections in the absence of normal outer retinal inputs.[64] Considering the order of retinal development, it seems most likely that normal numbers of sbRGCs develop and differentiate prior to the aberrant specification of photoreceptor fate in ESCS and that the excess S-cones in these retinas instead gain access to other retinogeniculate pathways with higher spatial resolution.

Direct Input to the Midget RGC Pathway. Could the supernormal S-cone acuity in ESCS subjects be mediated directly by the midget pathway? Midget RGCs primarily receive input from L- and M-cones and are widely believed to be the cell class mediating achromatic visual acuity across the visual field.[8,10–12] However, anatomical and physiological data from animal models indicate that a small portion of S-cone signals are also carried by the midget RGC pathway.[65–67] If the weak S-cone signal observed in mRGCs is due to the low proportion of S-cones in a normal eye, then it stands to reason that a larger proportion of S-cones would give rise to a proportional increase in that signal. In fact, our results indicate that S-cone acuity in ESCS starts to approach the L/M-cone–mediated acuities we obtained from our normal cohort at 4° eccentricity, suggesting that two functions might be limited by a common neural pathway in the band of eccentricities where S-cones may predominate in the ESCS retina.

Midget RGCs Via the Rod Pathway. In normal eyes, rod photoreceptors and rod bipolar cells gain access to the cone-driven ganglion cell pathway primary through the connection to the AII amacrine cells.[3] In patients with ESCS, multifocal ERG findings demonstrate a significant delayed b-wave in response to blue light, suggesting that the signals from the misdirected rod precursors may still feed into the relatively sluggish rod pathway.[53] This implication is supported by histological and electrophysiological evidence from the *nrl* knockout mice, which shows that the excess S-cones establish functional connections with conventional rod-driven circuits.[68]

The spatial resolution of rod-mediated vision across the central 15° to 20° of the retina matches the Nyquist sampling limit of the AII amacrine cells, the coarsest array in the rod pathway, with psychophysical measurements of rod grating acuity reported to be 5 to 7 cyc/deg at 5° eccentricity.[3,5] This is better than the normal S-cone grating acuity of 2 cyc/deg[13] and the averaged normal S-cone resolution acuity of 2.1 cyc/deg at 4° eccentricity found in our study. In addition, the AII sampling density increases with retinal eccentricity in the central retina, which aligns with the similar trend in the S-cone acuity found in our ESCS subjects (Fig. 5B). The AII amacrine cell array sampling limit could potentially support the supernormal S-cone acuity found in our ESCS subjects, which reached 5.6 cyc/deg at the 4° temporal retinal location.

The latter two hypotheses presented above require that S-cones in ESCS infiltrate retinal pathways ordinarily driven by L/M-cones. The strongest evidence to support this notion comes from a study in which a flicker perception task was used to examine the temporal characteristics of S-cone processing.[30] The critical flicker fusion (CFF) frequencies obtained from a cohort of patients with ESCS were consistent with a sluggish, but amplified, signal carried by the traditional S-cone pathway (i.e., sbRGCs) existing alongside a sizable, faster, phase-shifted component that could originate in a "luminance" pathway ordinarily driven by L/M-cones. Although the study authors did not speculate on the neural substrate of this achromatic pathway, physiological and psychophysical experiments have demonstrated that primate mRGCs are responsive to fast high-contrast flicker and could contribute psychophysical CFF measurements.[69,70] It is also noted that the authors of the temporal contrast sensitivity testing study[30] did not rule out the faster phase-shifted component in their temporal contrast sensitivity function as being due to the S-cones connecting to

the conventional rod pathway rather than via direct input. To distinguish between these two hypotheses, it would be of interest to measure S-cone–mediated acuity in an even younger cohort of ESCS subjects with little to no outer retinal degeneration. Within the central 5° to 20°, scotopic acuity is limited by the AII amacrine cell mosaic, whose spatial sampling is coarser than the mRGC mosaic.[3] If the S-cone acuity in early-stage ESCS mirrors the Nyquist sampling limit imposed by the AII amacrine cells across the parafovea, it would support the hypothesis that the conventional rod pathway provides an alternate conduit for S-cone signals in ESCS.

How Could We Learn More?

Previous structural analyses of ESCS retinas showed an absence of rods, but cones (presumably S-cones) were the dominant cone type in retinal areas outside of the fovea.[26–28] Our structural and functional results further establish that S-cones are in the majority in the parafoveal retina in ESCS. To objectively confirm the abnormal distribution of the L/M- and S-cone photoreceptors in ESCS eyes, however, a retinal densitometry[71,72] or an optoretinogram-based cone classification method[73,74] could be used. In addition to providing a cellular-scale spectral classification of the outer retina, optoretinography could also be used to characterize the responsivity of individual cones to light flashes,[75] which could aid in directly assaying cellular dysfunction that might be difficult to reveal psychophysically due to potential compensatory adaptations in post-receptoral circuits.

Further study is also needed to confirm the exact retinal wiring that supports the supernormal S-cone acuity we observed in patients with ESCS. New retinal connectomics tools such as serial block-face scanning electron microscopy have been used to elucidate the functional connectivity between cone photoreceptors and their downstream synaptic partners.[9,76–78] Similar techniques could be applied to ESCS donor tissue to determine whether the abundant S-cone signal is primarily conveyed by an increased number of sbRGCs (which can be readily identified by their morphology), if those short-wavelength signals instead infiltrate ordinarily L/M-cone–driven pathways with higher spatial resolution (i.e., mRGCs), or if novel wiring schemes emerge in the presence of a highly atypical set of outer retinal inputs.

In this study, we used a blue-on-yellow procedure to measure S-cone–isolated visual acuity. Although the long-wavelength adapting field is effectively unabsorbed by the S-cone opsin, it can indirectly influence S-cone signals by polarizing cone-opponent circuits downstream, leading to perceptual phenomena such as transient tritanopia[79,80] and changes in the shape of the S-cone contrast sensitivity function (CSF) with increasing background intensity.[81–83] Although transient tritanopia has been demonstrated in ESCS,[84] the extent to which S-cone–mediated spatial vision depends on the adaptation state of L- and M-cones is unknown. Examining the S-cone CSF across a range of background intensities may provide additional insights into post-receptoral organization in ESCS.

In conclusion, ESCS subjects exhibited higher than normal S-cone density and supernormal S-cone acuity outside the fovea. The supernormal S-cone acuity in ESCS could indicate retinal plasticity during development where abnormally increased numbers of S-cones establish connectivity to the downstream pathways ordinarily driven by L/M-cones.

References

1. Yuodelis C, Hendrickson A. A qualitative and quantitative analysis of the human fovea during development. *Vision Res*. 1986;26(6):847–855.
2. Curcio CA, Sloan KR, Kalina RE, Hendrickson AE. Human photoreceptor topography. *J Comp Neurol*. 1990;292(4):497–523.
3. Lee SCS, Martin PR, Grünert U. Topography of neurons in the rod pathway of human retina. *Invest Ophthalmol Vis Sci*. 2019;60(8):2848.
4. Lennie P, Fairchild MD. Ganglion cell pathways for rod vision. *Vision Res*. 1994;34(4):477–482.
5. Wilkinson MO, Anderson RS, Bradley A, Thibos LN. Resolution acuity across the visual field for mesopic and scotopic illumination. *J Vis*. 2020;20(10):7.
6. Curcio CA, Allen KA, Sloan KR, et al. Distribution and morphology of human cone photoreceptors stained with anti-blue opsin. *J Comp Neurol*. 1991;312(4):610–624.
7. Schleufer S, Pandiyan VP, Bharadwaj P, Sabesan R. Crystalline arrangement of S-cones in the central human retina. *Invest Ophthalmol Vis Sci*. 2022;63(7):ARVO E-Abstract 2235–F0443.
8. Rossi EA, Roorda A. The relationship between visual resolution and cone spacing in the human fovea. *Nat Neurosci*. 2010;13(2):156–157.
9. Zhang C, Kim YJ, Silverstein AR, et al. Circuit reorganization shapes the developing human foveal midget connectome toward single-cone resolution. *Neuron*. 2020;108(5):905–918.e3.
10. Thibos LN, Cheney FE, Walsh DJ. Retinal limits to the detection and resolution of gratings. *J Opt Soc Am A*. 1987;4(8):1524–1529.
11. Marcos S, Navarro R. Determination of the foveal cone spacing by ocular speckle interferometry: limiting factors and acuity predictions. *J Opt Soc Am A*. 1997;14(4):731–740.
12. Williams DR, Coletta NJ. Cone spacing and the visual resolution limit. *J Opt Soc Am A*. 1987;4(8):1514–1523.
13. Anderson RS, Zlatkova MB, Demirel S. What limits detection and resolution of short-wavelength sinusoidal gratings across the retina? *Vision Res*. 2002;42(8):981–990.
14. Sekiguchi N, Williams DR, Brainard DH. Efficiency in detection of isoluminant and isochromatic interference fringes. *J Opt Soc Am A Opt Image Sci Vis*. 1993;10(10):2118–2133.

15. Dacey DM. Morphology of a small-field bistratified ganglion cell type in the macaque and human retina. *Vis Neurosci.* 1993;10(6):1081–1098.

16. Marmor M. Large rod-like photopic signals in a possible new form of congenital night blindness. *Doc Ophthalmol.* 1989;71(3):265–269.

17. Jacobson SG, Marmor MF, Kemp CM, Knighton RW. SWS (blue) cone hypersensitivity in a newly identified retinal degeneration. *Invest Ophthalmol Vis Sci.* 1990;31(5):827–838.

18. Marmor MF, Jacobson SG, Foerster MH, Kellner U, Weleber RG. Diagnostic clinical findings of a new syndrome with night blindness, maculopathy, and enhanced s cone sensitivity. *Am J Ophthalmol.* 1990;110(2):124–134.

19. Audo I, Michaelides M, Robson AG, et al. Phenotypic variation in enhanced S-cone syndrome. *Invest Ophthalmol Vis Sci.* 2008;49(5):2082–2093.

20. Roman AJ, Powers CA, Semenov EP, et al. Short-wavelength sensitive cone (S-cone) testing as an outcome measure for NR2E3 clinical treatment trials. *Int J Mol Sci.* 2019;20(10):2497.

21. Garafalo AV, Calzetti G, Cideciyan AV, et al. Cone vision changes in the enhanced S-cone syndrome caused by NR2E3 gene mutations. *Invest Ophthalmol Vis Sci.* 2018;59(8):3209–3219.

22. Corbo JC, Cepko CL. A hybrid photoreceptor expressing both rod and cone genes in a mouse model of enhanced S-cone syndrome. *PLoS Genet.* 2005;1(2):e11.

23. Coppieters F, Leroy BP, Beysen D, et al. Recurrent mutation in the first zinc finger of the orphan nuclear receptor NR2E3 causes autosomal dominant retinitis pigmentosa. *Am J Hum Genet.* 2007;81(1):147–157.

24. Littink K, Stappers P, Riemslag F, et al. Autosomal recessive NRL mutations in patients with enhanced S-cone syndrome. *Genes (Basel).* 2018;9(2):68.

25. Mears AJ, Kondo M, Swain PK, et al. Nrl is required for rod photoreceptor development. *Nat Genet.* 2001;29(4):447–452.

26. Milam AH, Rose L, Cideciyan AV, et al. The nuclear receptor NR2E3 plays a role in human retinal photoreceptor differentiation and degeneration. *Proc Natl Acad Sci USA.* 2002;99(1):473–478.

27. Ammar MJ, Scavelli KT, Uyhazi KE, et al. Enhanced S-cone syndrome: visual function, cross-sectional imaging, and cellular structure with adaptive optics ophthalmoscopy. *Retin Cases Brief Rep.* 2021;15(6):694–701.

28. Roorda A, Sundquist S, Solovyev A, et al. Adaptive optics imaging reveals supernormal cone density in enhanced S-cone syndrome. *Invest Ophthalmol Vis Sci.* 2010;51(13):ARVO E-Abstract 2934.

29. Greenstein VC, Zaidi Q, Hood DC, Spehar B, Cideciyan AV, Jacobson SG. The enhanced S cone syndrome: an analysis of receptoral and post-receptoral changes. *Vision Res.* 1996;36(22):3711–3722.

30. Ripamonti C, Aboshiha J, Henning GB, et al. Vision in observers with enhanced S-cone syndrome: an excess of S-cones but connected mainly to conventional S-cone pathways. *Invest Ophthalmol Vis Sci.* 2014;55(2):963.

31. Haider NB, Demarco P, Nystuen AM, et al. The transcription factor *Nr2e3* functions in retinal progenitors to suppress cone cell generation. *Vis Neurosci.* 2006;23(6):917–929.

32. Nakamura PA, Tang S, Shimchuk AA, Ding S, Reh TA. Potential of small molecule-mediated reprogramming of rod photoreceptors to treat retinitis pigmentosa. *Invest Ophthalmol Vis Sci.* 2016;57(14):6407.

33. Upadhyay AK, Datta S, Brabbit E, Love Z, Haider NB, Arumugham R. Preclinical efficacy of AAV5-*Nr2e3* in the mouse model of *Nr2e3* mutation associated inherited retinal degeneration. *Invest Ophthalmol Vis Sci.* 2020;61(7):4466.

34. Ferris FL, Kassoff A, Bresnick GH, Bailey I. New visual acuity charts for clinical research. *Am J Ophthalmol.* 1982;94(1):91–96.

35. Cole BL. Assessment of inherited colour vision defects in clinical practice. *Clin Exp Optom.* 2007;90(3):157–175.

36. Wang Y, Bensaid N, Tiruveedhula P, Ma J, Ravikumar S, Roorda A. Human foveal cone photoreceptor topography and its dependence on eye length. *eLife.* 2019;8:e47148.

37. Duncan JL, Zhang Y, Gandhi J, et al. High-resolution imaging with adaptive optics in patients with inherited retinal degeneration. *Invest Ophthalmol Vis Sci.* 2007;48(7):3283–3291.

38. Stevenson SB, Roorda A, Kumar G. Eye tracking with the adaptive optics scanning laser ophthalmoscope. In: *Proceedings of the 2010 Symposium on Eye-Tracking Research and Applications.* New York: Association for Computing Machinery; 2010:195–198.

39. Chen M, Cooper RF, Han GK, Gee J, Brainard DH, Morgan JI. Multi-modal automatic montaging of adaptive optics retinal images. *Biomed Opt Express.* 2016;7(12):4899–4918.

40. Cooper RF, Wilk MA, Tarima S, Carroll J. Evaluating descriptive metrics of the human cone mosaic. *Invest Ophthalmol Vis Sci.* 2016;57(7):2992.

41. Duncan JL, Liang W, Maguire MG, et al. Change in cone structure over 24 months in USH2A-related retinal degeneration. *Am J Ophthalmol.* 2023;252:77–93.

42. Coates DR, Chung STL. Crowding in the S-cone pathway. *Vision Res.* 2016;122:81–92.

43. Watson AB, Pelli DG. QUEST: a Bayesian adaptive psychometric method. *Percept Psychophys.* 1983;33(2):113–120.

44. Prins N, Kingdom FAA. Applying the model-comparison approach to test specific research hypotheses in psychophysical research using the Palamedes toolbox. *Front Psychol.* 2018;9:1250.

45. Brainard DH. The Psychophysics Toolbox. *Spat Vis.* 1997;10(4):433–436.

46. Castet E, Crossland M. Quantifying eye stability during a fixation task: a review of definitions and methods. *Seeing Perceiving.* 2012;25(5):449–469.

47. Bowers NR, Gautier J, Lin S, Roorda A. Fixational eye movements in passive versus active sustained fixation tasks. *J Vis.* 2021;21(11):16.

48. Jacobson SG, Sumaroka A, Aleman TS, et al. Nuclear receptor *NR2E3* gene mutations distort human retinal laminar architecture and cause an unusual degeneration. *Hum Mol Genet.* 2004;13(17):1893–1902.

49. Yzer S, Barbazetto I, Allikmets R, et al. Expanded clinical spectrum of enhanced S-cone syndrome. *JAMA Ophthalmol.* 2013;131(10):1324–1330.

50. de Carvalho ER, Robson AG, Arno G, Boon CJF, Webster AA, Michaelides M. Enhanced S-cone syndrome: spectrum of clinical, imaging, electrophysiologic, and genetic findings in a retrospective case series of 56 patients. *Ophthalmol Retina.* 2021;5(2):195–214.

51. Anderson SJ, Mullen KT, Hess RF. Human peripheral spatial resolution for achromatic and chromatic stimuli: limits imposed by optical and retinal factors. *J Physiol.* 1991;442(1):47–64.

52. Shah N, Dakin SC, Redmond T, Anderson RS. Vanishing optotype acuity: repeatability and effect of the number of alternatives. *Ophthalmic Physiol Opt.* 2011;31(1):17–22.

53. Marmor MF, Tan F, Sutter EE, Bearse MA, Jr. Topography of cone electrophysiology in the enhanced S cone syndrome. *Invest Ophthalmol Vis Sci.* 1999;40(8):1866–1873.

54. Hood DC, Cideciyan AV, Roman AJ, Jacobson SG. Enhanced S cone syndrome: evidence for an abnormally large number of S cones. *Vision Res.* 1995;35(10):1473–1481.

55. Sohn EH, Chen FK, Rubin GS, Moore AT, Webster AR, Maclaren RE. Macular function assessed by microperimetry

in patients with enhanced S-cone syndrome. *Ophthalmology*. 2010;117(6):1199–1206.e1.

56. O'Brien KMB, Cheng H, Jiang Y, Schulte D, Swaroop A, Hendrickson AE. Expression of photoreceptor-specific nuclear receptor *NR2E3* in rod photoreceptors of fetal human retina. *Invest Ophthalmol Vis Sci*. 2004;45(8):2807.

57. Hendrickson A, Bumsted-O'Brien K, Natoli R, Ramamurthy V, Possin D, Provis J. Rod photoreceptor differentiation in fetal and infant human retina. *Exp Eye Res*. 2008;87(5):415–426.

58. Swaroop A, Kim D, Forrest D. Transcriptional regulation of photoreceptor development and homeostasis in the mammalian retina. *Nat Rev Neurosci*. 2010;11(8):563–576.

59. Zlatkova MB, Coulter E, Anderson RS. Short-wavelength acuity: blue-yellow and achromatic resolution loss with age. *Vision Res*. 2003;43(1):109–115.

60. Redmond T, Zlatkova MB, Vassilev A, Garway-Heath DF, Anderson RS. Changes in Ricco's area with background luminance in the S-cone pathway. *Optom Vis Sci*. 2013;90(1):66–74.

61. Dacey DM, Lee BB. The "blue-on" opponent pathway in primate retina originates from a distinct bistratified ganglion cell type. *Nature*. 1994;367(6465):731–735.

62. Dunn FA, DellaSantina L, Parker ED, Wong ROL. Sensory experience shapes the development of the visual system's first synapse. *Neuron*. 2013;80(5):1159–1166.

63. Xu H, Tian N. Pathway-specific maturation, visual deprivation, and development of retinal pathway. *Neuroscientist*. 2004;10(4):337–346.

64. Mazzoni F, Novelli E, Strettoi E. Retinal ganglion cells survive and maintain normal dendritic morphology in a mouse model of inherited photoreceptor degeneration. *J Neurosci*. 2008;28(52):14282–14292.

65. Klug K, Herr S, Ngo IT, Sterling P, Schein S. Macaque retina contains an S-cone OFF midget pathway. *J Neurosci*. 2003;23(30):9881–9887.

66. Field GD, Gauthier JL, Sher A, et al. Functional connectivity in the retina at the resolution of photoreceptors. *Nature*. 2010;467(7316):673–677.

67. Patterson SS, Kuchenbecker JA, Anderson JR, et al. An S-cone circuit for edge detection in the primate retina. *Sci Rep*. 2019;9(1):11913.

68. Bush RA, Tanikawa A, Zeng Y, Sieving PA. Cone ERG changes during light adaptation in two all-cone mutant mice: implications for rod-cone pathway interactions. *Invest Ophthalmol Vis Sci*. 2019;60(10):3680.

69. Merigan WH, Maunsell JHR. Macaque vision after magnocellular lateral geniculate lesions. *Vis Neurosci*. 1990;5(4):347–352.

70. Lee BB, Martin PR, Valberg A. Sensitivity of macaque retinal ganglion cells to chromatic and luminance flicker. *J Physiol*. 1989;414(1):223–243.

71. Roorda A, Williams DR. The arrangement of the three cone classes in the living human eye. *Nature*. 1999;397:520–522.

72. Sabesan R, Hofer H, Roorda A. Characterizing the human cone photoreceptor mosaic via dynamic photopigment densitometry. *PLoS One*. 2015;10(12):e0144891.

73. Pandiyan VP, Maloney-Bertelli A, Kuchenbecker JA, et al. The optoretinogram reveals the primary steps of phototransduction in the living human eye. *Sci Adv*. 2020;6(37):eabc1124.

74. Zhang F, Kurokawa K, Lassoued A, Crowell JA, Miller DT. Cone photoreceptor classification in the living human eye from photostimulation-induced phase dynamics. *Proc Natl Acad Sci USA*. 2019;116(16):7951–7956.

75. Lassoued A, Zhang F, Kurokawa K, et al. Cone photoreceptor dysfunction in retinitis pigmentosa revealed by optoretinography. *Proc Natl Acad Sci USA*. 2021;118(47):e2107444118.

76. Wool LE, Packer OS, Zaidi Q, Dacey DM. Connectomic identification and three-dimensional color tuning of S-OFF midget ganglion cells in the primate retina. *J Neurosci*. 2019;39(40):7893–7909.

77. Patterson SS, Mazzaferri MA, Bordt AS, Chang J, Neitz M, Neitz J. Another Blue-ON ganglion cell in the primate retina. *Curr Biol*. 2020;30(23):R1409–R1410.

78. Patterson SS, Kuchenbecker JA, Anderson JR, Neitz M, Neitz J. A color vision circuit for non-image-forming vision in the primate retina. *Curr Biol*. 2020;30(7):1269–1274.e2.

79. Stiles WS. Increment thresholds and the mechanisms of colour vision. *Doc Ophthalmol*. 1949;3(1):138–165.

80. Mollon JD, Polden PG. An anomaly in the response of the eye to light of short wavelengths. *Philos Trans R Soc Lond B Biol Sci*. 1977;278(960):204–240.

81. Stromeyer CF, Kronauer RE, Madsen JC. Adaptive processes controlling sensitivity of short-wave cone pathways to different spatial frequencies. *Vision Res*. 1984;24(8):827–834.

82. Humanski RA, Wilson HR. Spatial frequency mechanisms with short-wavelength-sensitive cone inputs. *Vision Res*. 1992;32(3):549–560.

83. Swanson WH. S-cone spatial contrast sensitivity can be independent of pre-receptoral factors. *Vision Res*. 1996;36(21):549–560.

84. Kellner U, Zrenner E, Sadowski B, Foerster MH. Enhanced S cone sensitivity syndrome: long-term follow-up, electrophysiological and psychophysical findings. *Clin Vis Sci*. 1993;8(5):425–434.

85. Stockman A, Sharpe LT. The spectral sensitivities of the middle- and long-wavelength-sensitive cones derived from measurements in observers of known genotype. *Vision Res*. 2000;40(13):1711–1737.